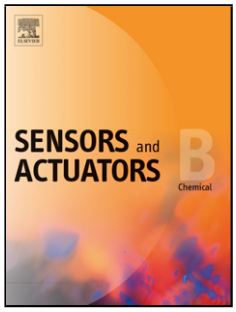

Title: Dynamic response of ammonia sensors constructed from polyaniline nanofibre films with varying morphology

Author: Plamen Stamenov Rethi Madathil J.M.D. Coey<ce:footnote id="fn0005"></ce:footnote>

PII: S0925-4005(11)01087-2
DOI: doi:10.1016/j.snb.2011.11.082
Reference: SNB 13661

To appear in: *Sensors and Actuators B*

Received date: 12-9-2011
Revised date: 28-11-2011
Accepted date: 29-11-2011

Please cite this article as: P. Stamenov, R. Madathil, J.M.D. Coey, Dynamic response of ammonia sensors constructed from polyaniline nanofibre films with varying morphology, *Sensors and Actuators B: Chemical* (2010), doi:10.1016/j.snb.2011.11.082

Dynamic response of ammonia sensors constructed from polyaniline nanofibre films with varying morphology

Plamen Stamenov, Rethi Madathil[1] and J. M. D. Coey
School of Physics & CRANN, Trinity College, Dublin 2, Ireland

Abstract:

Polyaniline is acid-doped with HCl, HNO_3, $HClO_4$, HBr or H_2SO_4 to yield thin films that are nanofibrous or dense. The nanofibrous films show a faster response to ammonia gas, and the response is greater when the films are in the moderately-conducting green state than when they are in the highly-conducting yellow state. The film resistance and optical absorption spectrum are monitored at 20 ms and 500 ms intervals, respectively during and after exposure to ammonia. Three absorption processes with characteristic times of order 10 s, 100 s, and 1000 s are observed in the resistive response. The optical spectrum is fitted with three Gaussians or derived Gaussians centred in the blue, orange and infra-red which exhibit similar response times of order 100 s and 1000 s, corresponding to the longer times in the resistive response. The data are interpreted in terms of three processes, physisorption, chemisorption and structural rearrangement of the polymer chains. Gas selectivity is demonstrated in the optical response by comparing the time-dependent desorption of H_2O and NH_3. These two gasses may be distinguished using inexpensive on-chip two band pass filter optical detection.

Keywords:

Polyaniline, nanofibres, ammonia sensor, chemristor, chemisorption, sensor dynamics.

[1] Current Address: Oxford Brooks University

1. Introduction

Gas sensors are important for many industrial, medical and commercial applications. There is an interest in developing devices that are simple and cheap to fabricate, which exhibit a reproducible and reversible response to gases such as ammonia [1] over a wide range of partial gas pressures. The sensors should be stable in ambient conditions. Thin film sensors made from conducting polymers [2] have the potential to meet these requirements [3, 4].

There are several distinct principles of sensor operation. The simplest and most commonly-used configuration is the 'chemristor', where the electrical conductance of a sensitive area of a thin film changes in the presence of the analyte. Variants of the resistor are the *p-n* junction, the Schottky barrier, capacitors and field-effect transistors where the organic film forms the channel or the gate. The optical spectrum of the polymer is also sensitive to changes of electronic structure caused by the analyte. Optical absorption may be measured directly in the UV, visible or infra-red regions, or else the polymer may be used as cladding on an optical waveguide. Mechanical sensor principles include measurement of the sound velocity in surface acoustic wave devices, or the influence of the change of mass on the resonant frequency of a quartz crystal or a silicon cantilever. Electrochemical sensors register a change of current-density at a polymer-modified electrode surface.

Here we are interested in polyaniline (PAni) films, which have potential as ammonia sensors based on conductivity [3-9] or optical transmission [4, 10-13]. We compare the dynamic electrical and optical responses of a series of conducting films with different resistances and morphologies. Conductivity of polyanaline varies greatly with the state of oxidation or protonation of the polymer [2]. The half-oxidized state, known as emeraldine base, is composed of alternating oxidized and reduced repeat units with a benzoid:quinoid ratio of 3:1 as shown in Fig 1. This insulating polymer becomes conducting when in a protonated, acid form [14], known as emeraldine salt. Salts can be formed from different acids, and their conductivity is related to the degree of order and morphology [15-20]. The best conductivity is found for HCl. The conduction in proton-doped polymers is not achieved by changing the number of π electrons on the polymer backbone, but by removing impediments to their delocalization as the protonated polymer undergoes structural relaxation with redistribution of charge to eliminate the quinoid groups, as shown in Fig. 1. A structure with alternating single and double bonds is necessary for the formation of delocalized electronic states.

Most conducting polymers are *p*-type semiconductors, but in the case of PAni, the conducting salts were thought to be metals, with sufficient overlap between oriented polymer chains to create a three-dimensional structure. The thermally-activated conduction found in even the most conducting

samples is then associated with tunnelling contacts between metallic grains [21]. The conducting polymer behaves like a granular metal. There is an electronic heat capacity and Pauli susceptibility [22], and tunnelling contacts between the metallic regions has been suggested as the origin of the variation of the conductivity as

$$\sigma = \sigma_\infty \exp\left(T / T_0\right)^{-1/2} \qquad (1)$$

which is typical of a granular metal [23]. The conductivity of the best-ordered PAni is of order 1000 S cm^{-1}, which is a factor of ten less than that of a normal amorphous or poorly-conducting metal. Conductivity may be increased by stretching the sample [24], or by secondary doping.

Chemristor sensors based on PAni require films that are electrically continuous, but permeable to gas. Since the material cannot be evaporated and is difficult to dissolve (with limited solubility in DBSA, isopropyl alcohol, toluene and xilene, of typically less than 3 %) [32], films have to be grown directly on a substrate by chemical or electrochemical polymerization methods. The response time of PAni thin film sensors on exposure to ammonia gas is fairly long, in the range 10 – 1000 s [4]. Hu et al [10,11] have analysed the time and pressure dependence of the optical transmission at a fixed wavelength of 632 nm. The time dependence of the transmission *T* following an abrupt change of gas pressure *P* is usually fitted to a sum of two or more exponentials:

$$\Delta T / T_0 = \sum_i A_i \left[1 - \exp\left(-\frac{t - t_0}{\tau_i^A}\right)\right] \qquad (2)$$

for absorption and

$$\Delta T / T_0 = \sum_i D_i \left[\exp\left(-\frac{t - t_0}{\tau_i^D}\right)\right] \qquad (3)$$

for desorption. Hu et al found that the characteristic times for absorption and desorption were similar, with pressure-dependent times $\tau_1 \approx 100$ s and $\tau_2 \approx 1000$ s , which were associated with two different absorption sites in the PAni surface. Activation energies at the two sites were similar, ≈ 0.8 eV. In this work, the changes in resistance (or resistivity) accompanying the absorption and desorption processes $\Delta R / R_0$ are analysed using the same exponential relations. Whenever unnormalized values of A_i and D_i are quoted in the text, their units are stated explicitly as Ω for the resistive responce data, or are implicitly taken as 12-bit amplitude values (to be normalized by 4096) for the optical absorption responce.

Analysis of the absorption isotherms at different pressures, using the Langmuir expression for the coverage fraction:

$$\theta = \sum_i \frac{\alpha_i \left(P^{1/n_i} \right)}{1 + \alpha_i \left(P^{1/n_i} \right)} \tag{4}$$

which reduces to the Freundlich isotherm at low gas pressures gives values, for the activation energy of absorption and heat of reaction of 0.3 – 0.5 eV for the two sites [10, 11]. Hereafter the coefficients α_i are defined as:

$$\alpha_i = \gamma \left(\frac{\beta(P,T)}{\beta(P_0,T_0)} \right)^{1/n_i} \exp\left(-\frac{E_i}{k_B T} \right) \tag{5}$$

with the number of molecules per unit area and time, β stipulated as:

$$\beta = P / \sqrt{2\pi m k_B T} \tag{6}$$

and T_0 and P_0 being the standard reference temperature (here set at 300 K), and the equilibrium vapour pressure of the adsorbate gas at the standard temperature, respectively. E_i are the specific energies of sorption (normally negative quantities) and m is the mass of the adsorbate molecule. The remaining dimensionless free coefficients γ and n are used as fitting parameters, which depend on the surface morphology and the effective surface area, as well as the detailed mechanisms for adsorption, and any concurrent chemisorption processes.

The present study is aimed at exploring the ammonia response of PAni films of widely differing morphologies, measuring both the optical absorption and electrical conductivity as a function of time in the same films. We explore the influence of film morphology on the sensor response [16, 17], and discuss both the influence of ammonia on the electronic structure of the conducting polymer and the effect of moisture [25]. We show how the films may be used to sense the presence of ammonia and water vapour simultaneously.

2. **Sensor preparation and characterization**

Conducting PAni films were prepared following the two-pot synthesis method described elsewhere [26], which involves repeated oxidation and reduction. A substrate of mylar or borosilicate glass is alternately dipped in an oxidant (ammonium persulphate) and a reducing agent (aniline plus acid) to build up films of thickness of less than 1 μm. Five different inorganic acids were used: HCl, HNO_3, $HClO_4$, HBr and H_2SO_4. Each acid produced a characteristic morphology, illustrated in Fig. 2. PAni

doped with HCl, HNO_3 or $HClO_4$, exhibits an open texture, with connected fibres that are a few microns long, and about 200 nm in diameter; HBr or H_2SO_4 produced a rough, dense texture. Optical spectra of the HCl-doped flms shown in Fig. 3 are for the polyemeraldine salt, before and after secondary acid doping (with m-cresol), which has the effect of improving the order of the polymer chains and increasing the conductivity by two orders of magnitude to values as high as 2000 S cm^{-1}.

The resistance of small pieces of the films about 5 x 2 mm was measured by the conventional four-probe method, using gold contacts. The temperature dependence of the resistivity follows Eq. 1 from 10 – 300 K, as demonstrated on Fig. 4. The resistance of the film measured at 1.8 K (not shown) increases quadratically with applied magnetic field, with a change of 80% in a field of 5 T.

The films were exposed to the analyte, anhydrous 99.99 % pure ammonia gas, in a small chamber made from a KF40 cross, at room temperature. Chamber volume was kept small (~30 cm^3) in order to diminish the influence of the self-diffusion in ammonia gas at the highest pressures D_{11} ~ 0.44 cm^2/s [27]. The chamber was first evacuated from ambient atmospheric pressure, to base pressure, while monitoring the sample resistance (the characteristic time constant of this pump-out process is in all cases less than 1 s). Then, ammonia was introduced via a manually controlled needle valve to reach the required gas pressure, which is expressed as a fraction of atmospheric pressure in ppm. Mostly 500 ppm was used, however the actual pressure was monitored and recorded in real-time. The chamber was then evacuated again, and the dynamic desorption isotherm was measured. Resistance was monitored at 20 ms intervals during repeated exposure and vacuum cycles to establish the time-dependent isothermal sensor response and its reversibility. These ammonia exposures – vacuum exposures cycles we repeated a number of times, until sensor response has been roughly stabilised. Both absorption and desorption were monitored in a constant-flow control mode, i.e. upon a pressure transition, the control valve was set at the target flow-rate, while pressure was monitored, but not stabilised by any feedback, in order to avoid the generation of control oscillations of pressure as function of time. Therefore, the overall relative error of the gas pressure could reach about 5 %. Under the same gas handling conditions, the optical absorption spectra were measured using two different Ocean Optics multichannel CCD-based spectrometers S1000 and S2000 under broadband high-pressure Xe discharge illumination. The entire spectrum from 400 – 900 nm was monitored every 500 ms. A set of curves, showing the long-term response to different gases and pressures is shown on Fig. 5, for a film proton doped with HCl without secondary doping, and on Fig. 6, for a film with secondary doping.

3. Results

3.1 Resistive response.

Both dynamic absorption and desorption response is measured. For technical reasons, it is easier to stabilise ammonia gas pressure in the desorption, rather than in the absorption, part of a pressure cycle. A representative example of a fit of the dynamic desorption isotherm to an expression of the type (3) is shown on Fig. 7. Three different characteristic times can be extracted, together with the corresponding amplitude coefficients. Typical sample resistances were in the range 1-30 kΩ, for exposed nominal area of 12-17 mm^2, and conductivities 50-1000 S/m.

Table 1 gives the resistance of samples of the different proton doped PAni films (without secondary doping), together with the three different characteristic times and the corresponding amplitude coefficients, and the overall relative change in resistance, on desorption from a state saturated at 500 ppm of ammonia. Similar data, collected at the absorption part of ammonia pressure pulses, is summarised in Table 2. Here only two different characteristic times are resolvable. The longest characteristic time (of the order of 1000 s) is not measured, due to poor long term stability of the ammonia gas flow used. By comparing the overall relative resistive responses upon absorption and desorption, it should be noted that while the values are quite similar for every particular dopant, they are not identical with respect to experimental errors, due to the partially irreversible behaviour. The overall magnitude of the response of the virgin films to NH_3 gas can exceed 400 % per 500 ppm and is comparable and higher than other reports. [28] This is likely due to high energy chemisorprtion and structural rearrangement processes. The first two response times, τ_1 and τ_2 of the films with the open, fibrous structures are notably faster, and are affected to a lesser extent by irreversible processes, than those of the denser films. We therefore further focused our attention on sensors proton doped with HCl alone and additionally doped with m-cresol. A comparison of the resistive response of films with (yellow) and without secondary doping (green), is presented in Table 3.

An example of a very slow, close to thermodynamic equilibrium absorption isotherm is shown on Fig. 8. The behaviour is practically logarithmic at high concentrations as shown on the inset. A reasonable fit can be achieved to an adsorption-like model (such as Eq. 4), which results in an absorption activation energy of about 0.16(3) eV for the best-fit value of n of about 0.8, but it depends only slightly on whether n is fixed at unity or left as a free fitting parameter.

3.2 Optical response

The pre-processing of the raw real-time optical transmission data involves obtaining the difference spectrum by subtracting the unexposed (in-vacuum) absorption spectrum from the spectrum after exposure to ammonia, calculated at each 500 ms time point. It was fitted to three Gaussians, as illustrated in Fig 9. The narrow one, centred in the blue near 440 nm, represents an increase of optical absorption due to ammonia, whereas the broad one centred in the orange near 650 nm represents a decrease. The third, infrared component, at 840 nm, increases in the green films, but decreases in the yellow ones, where it is centred at a longer wavelength. This component is likely to be directly influenced by the concentration of weakly-localised polarons.[30] In this way we can follow the time response of different parts of the spectrum, fitting each component to Eq 2 or 3. Unlike the resistance, just two exponentials were required to fit the data, due to both the slower temporal response of the acquisition system and the lower relative accuracy. A typical fit for the lowest wavelength, blue component at 459 nm is shown in Fig 10, for a yellow film, where the characteristic times are 23 s and 243 s.

Table 4 lists the position and halfwidths of the three Gaussian components of the difference spectra. The components are practically the same for each of the three green films, and for each of the three yellow films, but they are shifted by 5 - 10% towards longer wavelengths in the more ordered yellow films. The intensities of these three components were then fitted with the double exponential decay, Eq 2. The two amplitudes and characteristic times for each component of the difference spectrum are shown in Table 5. The fitting is performed with fixed positions and widths of the spectral components, which is a good approximation for the case of NH_3 absorption. The values of the fitting parameters, obtained from this procedure, can be utilised to perform a more numerically unstable fitting with free spectral features. The results of such a data processing process are summarised in Table S1.

The corresponding amplitudes are of comparable magnitude for each spectral component. The characteristic times of the short time response is about 20 s, and that of the long time response is a few hundred seconds. These times are usually longer in the green films than in their yellow counterparts. They appear to correspond to the medium and long time responses detected in the resistivity measurements. The shortest characteristic time seen in resistivity could not be observed properly in the optical absorption, due to the order of magnitude longer acquisition times.

The time-evolution of the wavelengths of the three spectral components for a green sample are shown in Fig 11. These may be attributed to chemisorptive processes and stuctural rearrangements, and their kinetics is more difficult to quantify. It is clearly noticeable, however, that their dynamic

response is far less reversible, with a systematic long-time trend. The amplitudes of the spectral features exhibit typically smaller level of irreversibility (< 20 %), even for green films with relatively large response magnitude. An illustration is shown on Fig 12, for a green sample. Three-dimensional images of the ammonia data sets are presented in Fig 13. In these examples, the ammonia pulse ($c \approx 500$ ppm) was initiated at $t = 0$ s and finished at $t = 500$ s. The magnitude of the relative response peaks to about 45 % for the green films, and about 7.5 % for the yellow ones.

3.3 Water vapour.

The change in resistivity and optical absorption were monitored during evacuation of the sample chamber. They are largely attributed to a change of the relative humidity of the ambient environment from ~50 % to zero. The typical increase in relative resistance was in the range 150-500 %, depending on acid doping. The average increase for HCl-doped films was 180 %, reducing to about 115 %, upon co-doping with m-cresol. The resistive response has sign opposite to the one measured upon ammonia absorption and is substantially (often more than 1000 times, when the absolute concentration of the analyte is taken into account) less sensitive. A detailed study of the absorption/desorption kinetics, in resistive response, was not undertaken because the relative smallness of the observed effects and the technical problems associated with providing large and abrupt step-changes in water vapour pressure would have prevented the extraction of the shortest characteristic times.

An optical absorption difference spectrum of a green film in the two states is shown in Fig 14. Table 6 shows the components of the fits to the difference spectra, and Table 7 gives the time dependence. In all tables (d) is used to denote derived Gaussian spectral components. These are used to account for the small displacement of absorption features, as well as the high derivatives observed in certain regions of the raw absorption spectra, in particular, the absorption bands just below 450 nm. The same protocol is used for the spectral fitting – at first fixed spectral features position and widths are used (only amplitudes are extracted), which are then released, on expense of numerical stability and signal-to-noise ratio, in order to extract the temporal behaviour of all parameters. A summary of these results, analogous to Table S1, is presented in Table S2. The time evolution of positions and widths are more difficult to process, even in cases when the changes in wavelengths are sizable. Typical absolute displacements were a few nanometres, but could exceed 50 nm, in some cases. The values of the wavelength shifts and the corresponding time constants, which could be reliably extracted, are presented in Table S3. In some cases the changes in the widths of the spectral

features could also be recovered in a statistically justifiable fashion. The same are summarised in Table S4. Some of the time constants observed are in the thousands of seconds and clearly point towards significant energy barrier for chemisorption on at least one characteristic site. The shortest characteristic times extracted are of the order of few seconds and are likely associated with the removal of physisorbed water. Finally, the three-dimensional data sets for H_2O data on yellow and green films are summarized in Fig 15.

4. Discussion

We first discuss briefly the conduction mechanism in the PAni films. Although some of our yellow films are highly conducting, with resistivities as low as ~500 μΩ cm which approach those of poor metals, it seems that the thermally activated conduction is an intrinsic property of the polymer. It is not a property dominated by tunnel contacts between regions with truly metallic conduction. The evidence for this is the similar time constants for the optical and resistive responses. The entire optical spectrum changes on exposure to ammonia, which would not be the case if it were only intergranular contacts that are involved. The temperature dependence of the conductivity illustrated in Fig. 4 is plausibly explained by hopping of weakly-localized polarons along the one-dimensional polyaniline chains.

As regards the benefits of a fibrous PAni morphlogy for sensors [17, 31], the studies show that the fibrous films produced using our synthesis method [26] have a much faster response time and exhibit similar stability and changes in electrical resistance to the dense films. There is a trade-off to be made between porosity and speed, and lower magnitude but better reproducibility of the response. This is illustrated in the appendix on Fig A1. Depending on the particular acid doping, the films show either very large response up to 400 % per 500 ppm of NH3, with a substantial degradation of about a factor of 2 in 5 cycles; or a more moderate response of over 200 % per 500 ppm, but reproducible down to a few per cent upon cycling. Films doped with HCl exhibit the highest response magnitudes, while H_2SO_4 doping results in the best long term stability. Co-doping the films, with HCl and m-cresol, results in a good compromise between high conductivity and stability and large magnitude of the sensor response. The interfibre contacts resulting from growth by repeated oxidation and reduction are not fragile.

The scheme by which ammonia interacts with PAni to modify its properties is sketched in Fig 16. Initially, the gas is physisorbed throughout the polymer. This has little effect on the optical spectrum, but modifies the potential seen by the hopping polarons. The next step is chemisorption,

with the formation of ani-ammonia complexes on the polymer. Finally, there is a slow response which is associated with rearrangement of the polymer structure and with deprotonation of the anaine sites. The spectral changes are similar to the ones seen on completion of the polymerisation process during film preparation.[29]

The times needed for rearrangement of the polymer structure are notably longer for the highly conducting, yellow films. This is understandable, since the structure of these films has already been modified and stabilized by the secondary doping.

A problem with thin film sensors made from conducting polymers is the unspecific nature of their response, especially for large magnitudes (> 400 % per 500 ppm of NH_3). For example, with a chemristor, it is not easy to distinguish between changes of resistance produced by relative humidity or ammonia. In our case, we find that the resistance change produced by 50 % humidity is roughly equivalent to that created by 100 ppm of NH_3 for the green films. Despite the lower response magnitudes of the yellow films, the relative ratios are similar. While optical response offers lower magnitude effects (< 45% per 500 ppm NH_3), and slightly higher sensitivity to H_2O vapour – resistance change due to 50 % humidity is roughly equivalent to the one for 200 ppm of NH_3. Since one of the larger applications for NH_3 sensors is leakage detection in ambient environment, the indiscriminate resistive response limits the long-term drift-limited measurement floor. The optical response offers better prospects, as there are two wavelength bands for the green films and one for the yellow films where the absorption is almost independent of ammonia concentration. By monitoring the optical response at different wavelengths, Fig 17, it is expected that it should be possible to achieve some limited selectivity.

5. **Conclusions**

Nanofibrous PAni thin films exhibit good characteristics for gas sensing; they show a large resistance change with no hysteresis and a fast response. Measurement of conductance and optical absorption in the same samples has allowed us to build up an understanding of processes relevant to ammonia sensing by these films. There is a rapid change or resistance related to physisorption of the gas, followed by a chemisorption step with kinetics associated with of formation of ani - ammonia complexes on the polymer, and modification of the infra-red-active vibration modes characteristic of localized polaron states. Finally, there is a slow response in the visible spectrum and in the resistance which is associated with structural rearrangements of the polymer linked with deprotonation of the anine sites. We have provided a complete data set with detailed fits on the optical response which is

more promising than the resistive response for sensor applications. Both the highly-conducting, yellow films and the less conducting, green ones may be used as sensors; the response of the more resistive, green films is greater and faster whereas that of the yellow films shows better reproducibility. The optical sensors may be inexpensively integrated onto a chip with appropriate light-emitting diodes and photodiodes.

Acknowledgements

This work was supported by Science Foundation Ireland as part of the MANSE project 05/IN/1850. The authors wish to thank Steve Watts and Robbie Hollingworth for help with some early aspects of the work.

Appendix

The long term stability and reproducibility of the sensor response is of great practical importance. It depends on both chemical and morphological details and can be controlled by acid doping post polimerisation. Examples of NH_3 pulsing sequences, as seen in resistive response, are shown on Fig A1. Is should be noted that for most films, the magnitude of the response, the vacuum background resistance or both change upon repetitive exposure. The H_2SO_4-doped polyaniline sensors show the best long-term stability and signal response reproducibility.

References

[1] B. Timmer, W. Olthuis and A van den Berg, Ammonia sensors and their applications — a review, Sensors and Actuators B **107** (2005) 666-677

[2] A. G. MacDiarmid, Synthetic metals: a novel role for organic polymers, Synthetic Metals **125** (2002) 11 - 22

[3] J. Janata and M. Josowicz, Conducting polymers in electronic chemical sensors, Nature Materials **2** (2002) 19 – 24

[4] H. Bai and G. Q. Shi, Gas sensors based on conducting polymers, Sensors **7** (2007) 267-307

[5] A. I Kukla, Y. M. Shirshov, S. I. Piletski, Ammonia sensors based on sensitive polyanaline films, Sensors and Actuators B **37** (1996) 135 - 140

[6] V. V. Chabukswar, S. Pethkar and A. A. Athawale, Acrylic acid doped polaniline as an ammonia sensor, Sensors and Actuators B **77** (2001) 767-663

[7] S. Virji, J. X. Huang, R. B. Kaner and B. H. Weiller, Polyaniline nanofiber gas sensors: Examination of response mechanisms, Nano Lett. **4** (2004) 491-496

[8] D. Nicolas-Debarnot and F. Poncin-Epaillard, Polyanaline as a new sensitive layer for gas sensors, Analytica Chimica Acta **475** (2003)1 - 15

[9] G. K. Prasad, T. P. Radhakrishnan, D. S. Kumar and M. G. Krishna, Ammonia sensing characteristics of thin film based on polyelectrolyte-templated polyaniline, Sens. Actuators B **106** (2005) 625-631

[10] M. E. Nicho, M. Trejo, A. Garcia-Valenzuela, F. M. Saniger, J. Palacios and H. Hu, Polyanaline composite coatings interrogated by a nulling optical ttranmission bridge for sensing low concentrations of ammonia gas, Sens. Actuators B **76** (2001) 18 - 24

[11] H. Hu, M. Trejo, M. E. Nicho, J. M. Sanger and A. Garcia-Valenzuela, Adsorption kinetics of optochemical NH_3 gas sensing with semiconductor polyaniline films, Sens. Actuators B **82** (2002) 14-23

[12] S. Christie, E. Scorsone, K. Persaud and F. Kvasnik, Remote detection of gaseous ammonia using the near-infrared transmission propoerties of polyanaline, Sens. Actuators B **90** (2003) 163 – 169

[13] Y. S. Lee, B. S Joo, N. K. Choi, J. O. Lim, J. S. Huh and D. D. Lee, Visible optical sensing of ammonia based on polyaniline film, Sens. Actuators B **93** (2003) 138 - 152

[14] J. Strejskal and R. G. Golbert, Polyaniline, Preparation of a conducting polymer, Pure Appl. Chem. **74** (2002) 857-867

[15] Z. M. Zhang, Z. X. Wei and M. X. Wan, Nanostructures of polyanaline doped with inorganic acids, Macromolecules **35** (2002) 5937-5942

[16] J. Huang, S. Virji, B. H. Weiler and R. B. Kaner, Polyanaline fibres: facile synthesis and chemical sensors, J. Amer. Chem. Soc. **125** (2003) 314-315

[17] G. F. Li, C. Martinez, J, Janata, J. A. Smith, M. Josowicz and S. Semancik, Effect of morphology on the response of polyaniline-based conducting gas sensors: nanofibers vs thin films, Electrochem. Solid State Lett, **7** (2004) H44-47

[18] N. Bohli, F. Gmati, A. Belhadj Mohamed, V. Vigneras and J. L. Miane, Conductivity mechanism of polyaniline organic films: the effects of solvent type and casting temperatures, J. Phys. D **42** (2009) 205404

[19] S. Sinha, S. Bhadra and D. Khastgir, Effect of dopant type on the properties of polyaniline, J. Appl. Polymer Sci. **112** (2009) 3135 - 3140

[20] M. X. Wan, Some issues related to polyanalyine micro/nanostructures, Macromolecular Rapid Communications **30** (2009) 963 – 975.

[21] Z. H. Wang, C. Li, E. M. Scherr, A. G. MacDiarmid and A. J. Epstein, Three dimensionality of metalic states in conducting polymers: polyanaline, Phys. Rev. Lett. **66** (1991) 1745-1749

[22] A. Ragahunathan, P. K. Kahol, J. C. Ho, Y. Y. Chen, Y. D. Hao, Y. S. Lin and B. Wessling, Phys. Rev. B **58** (1998) R15955-15958

[23] B. Abeles, P. Sheng, M. D. Coutts and Y. Arle, Structure and electrical properties of granular metal films, Advances Physics, **24** (1975) 407-461

[24] S. J. Pomfret, P. N. Adams, N. P. Comfort and A. P. Monkman, Electrical and mechanical properties of polyaniline fibres produced by a one-step wet spinning process, Polymer **41** (2000) 2265-2369

[25] M. Matsuguchi, A. Okamoto and Y. Sakai, Effect of humidity on NH_3 gas sensitivity of polyanaline blend films, Sens. Actuators B **94** (2003) 46-52

[26] R. Madathil, Multilayer growth of conductive polyaniline: A two pot, alternate oxidation and reduction strategy, Synthetic Metals, **150** (2005) 123-126

[27] C. E. Baker, Temperature dependence of self-diffusion coefficients for gaseous ammonia, NASA technical note, NASA TN D-5574

[28] N. G. Deshpande, Y. G. Gudage1, R. S. Devan, Y. R. Ma, Y. P. Lee and R. Sharma, Room-temperature gas sensing studies of polyaniline thin films deposited on different substrates, Smart. Mater. Struct. **18** (2009) 095010

[29] J. Stejskal, P. Kratochvil and N. Radhakrishnan, Polyaniline dispersions 2. UV-Vis absorption spectra, Synthetic Metals **61** (1993) 225-231

[30] Y. H. Kim, C. Foster, J. Chiang and A. J. Heeger, Photoinduced Localized Charged Exitations in Polyaniline, Synthetic Metals **26** (1988) 49-59

[31] H. Tai, Y. Jiang, G. Xie, J. Yu, X. Chen, Z. Ying, Influence of polymerization temperature on NH_3 response of PANI/TiO_2 thin film gas sensor, Sensors and Actuators B **129** (2008) 319-326

[32] I. Dumitrescu, C-Anicolae, A. M. Mocioiu, R. A. Gabor, M. Grigorescu, M. Mihailescu, Synthesis and characterisation of conductive polymers with enhanced solubility, U.P.B. Sci. Bull. A **71** (2009) 63-72

Profiles:

Plamen Stamenov is Assistant Professor (Ussher Lecturer in Nanoscience) in the School of Physics at Trinity College Dublin, and a Principal Investigator in CRANN, Ireland's nanoscience research center. His interests are centred on the electronic and magnetic properties of solids, physical measurements and instrumentation.

Rethi Madathil is a graduate of Cochin University of Science and Technology. She worked as a postdoctoral research fellow with the schools of Chemistry and Physics at Trinity College Dublin from 2002 to 2005. Her recent interests are in experimental and computational studies of ion selectivity in hemolysin mutants.

Michael Coey is Erasmus Smith's Professor of Natural and Experimental Philosophy at Trinity College Dublin. He was Deputy Director of CRANN from 2004- 2010. His research interests are in magnetism and magnetic materials, spin electronics, magnetoeelctrochemistry and magnetobiology. He was awarded the 2011 RDS/INTEL Prize for Nanoscience.

Table 1. Response characteristic times and amplitudes of films with different proton doping upon ammonia desorption.

Dopant	R_0 (Ω)	D_1 (Ω)	τ_1 (s)	D_2 (Ω)	τ_2 (s)	D_3 (Ω)	τ_3 (s)	$\Delta R/R_0$ (%)
HCl	17881	10218	46.4	6977	351.4	7163	2823	-136
$HClO_4$	3625	2773	38.43	2688	197.2	3177	1247	-238
HNO_3	22697	3636	31.65	3986	214.5	6012	1743	-60
H_2SO_4	2228.3	3688	10.56	1101	157.9	739	1393	-248
HBr	15798	3396	11.69	2784	64.31	4217	465	-66

Table 2. Response characteristic times and amplitudes of films with different proton doping upon ammonia absorption.

Dopant	R_0 (Ω)	A_1 (Ω)	τ_1 (s)	A_2 (Ω)	τ_2 (s)	A_3 (Ω)	τ_3 (s)	$\Delta R/R_0$ (%)
HCl	20046	-7340	16.5	-10178	218.8	--	--	87
$HClO_4$	3841	-363	12.9	-5639	209	--	--	156
HNO_3	24363	-5017	22.67	-8659	273.3	--	--	56
H_2SO_4	2411	-824	30.45	-3374	296.6	--	--	174
HBr	18605	-2624	6.58	-8288	109.4	--	--	59

Table 3. Response characteristic times and amplitudes of films proton-doped with HCl (G) and additionally doped with m-cresol (Y), for NH_3 desorption.

Sample	R_0 (Ω)	D_1(Ω)	τ_1(s)	D_2(Ω)	τ_2(s)	D_3(Ω)	τ_3(s)
Y2	2833	1607	17.0	1009	185	962	2520
Y1	3836	7896	4.2	272k	65	308k	1259
G2	132.6k	517.2k	10.9	617k	49	261k	216
G1	300.3k	3430k	2.0	1960k	17.5	375k	191

Table 4. Components of the fits to the difference spectra for NH_3 absorption

Sample	λ_1 (nm)	$\Delta\lambda_1$(nm)	λ_2 (nm)	$\Delta\lambda_2$(nm)	λ_3 (nm)	$\Delta\lambda_3$(nm)
G1	425.99	45.01	630.29	153.02	833.72	107.81
G2	426.4	45.24	632	148.37	843.06	108.94
G3	429.91	38.96	626.17	141.7	830.24	104.56
Y1	461.01	22.61	655.03	174.97	899.74	75.9
Y2	460.14	18.9	667.38	216.45	979.32	223.95
Y3	458.87	21.72	666.83	185.12	895	113.41

Table 5. Characteristic times of the three Gaussian components of the absorption spectra for NH_3 absorption with fixed spectral parameters.

Wavelength	λ_1				λ_2				λ_3			
Coefficient	A_1	τ_1	A_2	τ_2	A_1	τ_1	A_2	τ_2	A_1	τ_1	A_2	τ_2
G1	291	24.6	329	480	-1044	24.2	-716	299	2519	35.7	2238	398
G2	321	23.9	398	398	-839	18.6	-567	272	2468	20.7	2066	254
G3	385	35	515	530	-1272	29.3	-1463	358	4521	31.8	4775	351
Y1	64.9	24.1	49.85	297	-454	40	-483	390	-72	35	-285	1296
Y2	18.7	19	20.2	215	-315	25	-313	301	-243	57	-207	617
Y3	123	21.8	100	231	-1103	25.2	-958	326	-177	18	-464	683

Table 6. Components of the fits to the difference spectra for H_2O desorption.

Sample	λ_1 (nm)	$\Delta\lambda_1$(nm)	λ_2 (nm)	$\Delta\lambda_2$(nm)	λ_3 (nm)	$\Delta\lambda_3$(nm)
G1	445.9	34.6(d)	826	140.6(d)	781.2	38.6
G2	448.6	37.2(d)	808	108(d)	817	42
G3	445.2	33.2(d)	828	145.6(d)	771.1	32.2
Y1	437.5	38.6(d)	849	44(d)	810	54.7
Y2	445	58(d)	628	122(d)	764	95
Y3	446.6	49.2	764.2	95.6	629.5	61.3

Table 7. Characteristic times of the three Gaussian components of the optical absorption spectra for H_20 desorption with fixed spectral characteristics.

Wavelength	λ_1				λ_2				λ_3			
Coefficient	A_1	τ_1	A_2	τ_2	A_1	τ_1	A_2	τ_2	A_1	τ_1	A_2	τ_2
G1	-37(d)	10.1	--	--	-195(d)	7	-521(d)	324	-539	11.7	344	349
G2	-40.9(d)	13.6	55.2(d)	3004	308(d)	33	-463(d)	269	-1196	7.4	-429	115
G3	-68(d)	15.7	81.6(d)	5149	-319(d)	37	-687(d)	367	-1934	11.5	2249	3331
Y1	-171(d)	4.5	-128(d)	142	-6(d)	7.4	-12.8(d)	376	-55	59	--	--
Y2	-15(d)	10.2	9(d)	393	-49	5.4	68	392	-54	43	124	387
Y3	-24	6.1	-10	42	87	12	257	328	-133	14	-369	238

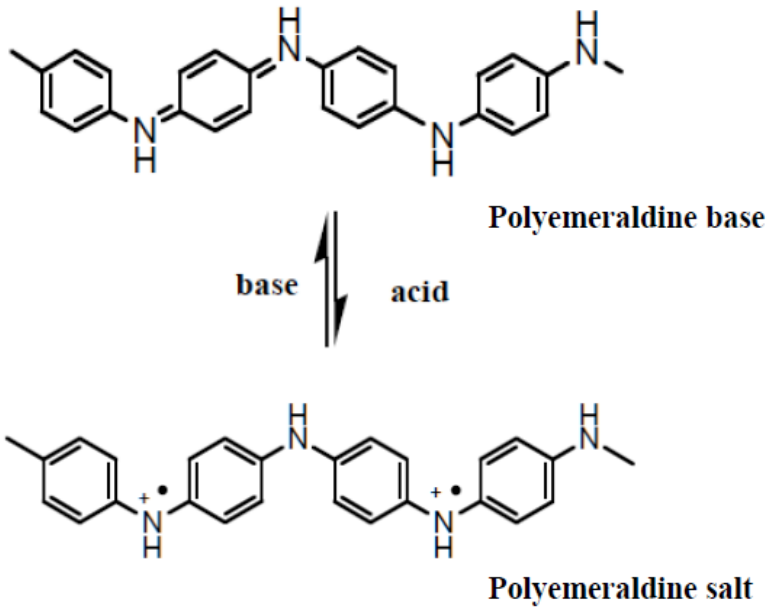

Figure 1. Proton doping of polyemeraldine with HCl.

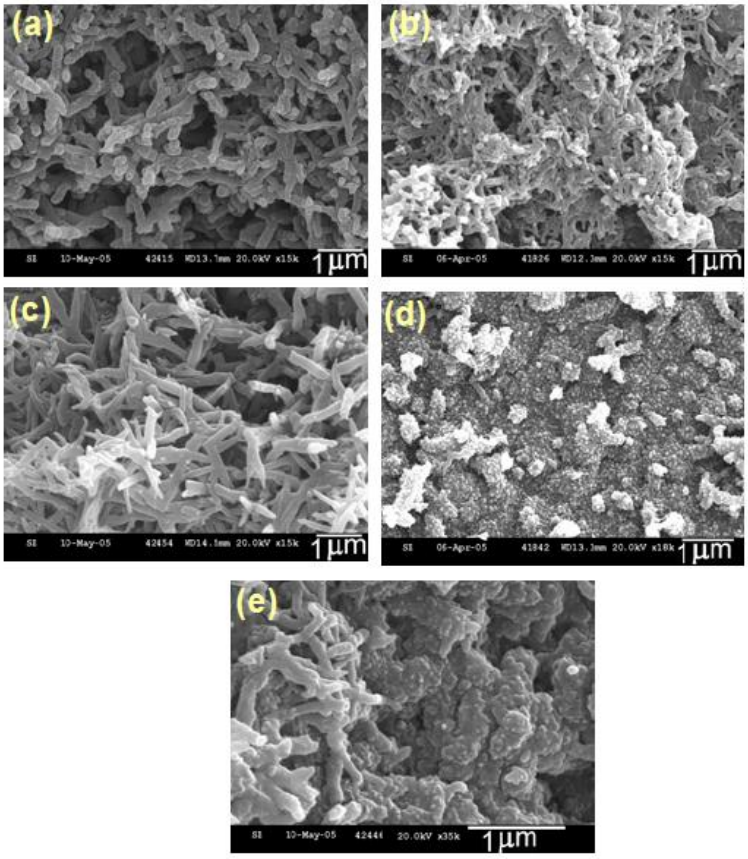

Figure 2. Scanning electron micrographs of PAni films doped with a) HCl, b) HNO_3, c) $HClO_4$, d) HBr and e) H_2SO_4.

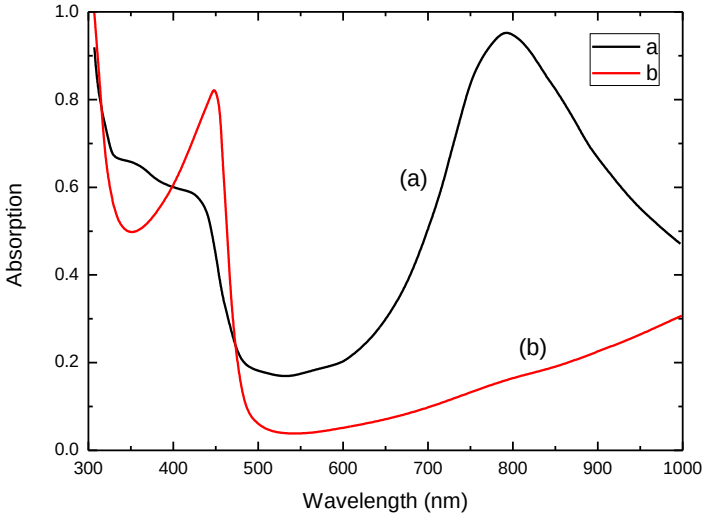

Figure 3. Optical spectra of green and yellow PAni (polyemeraldine) films proton doped with HCl a), before and b) after secondary acid doping.

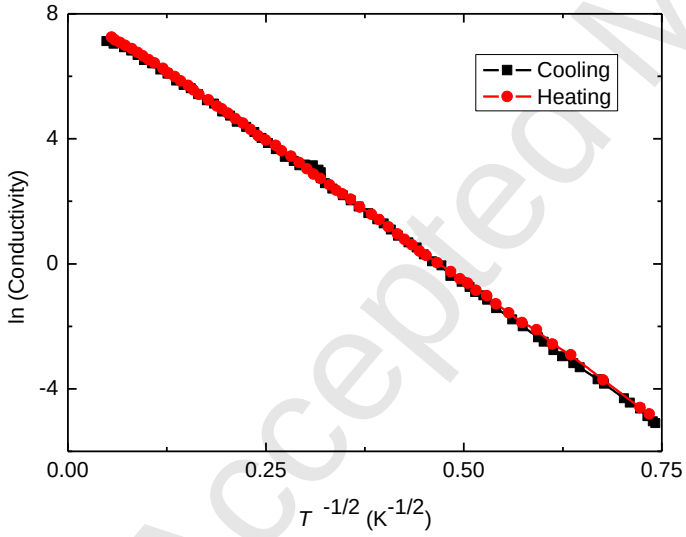

Figure 4. Temperature dependence of the resistivity of the PAni film of Fig 3b) measured on cooling (black) and heating (red).

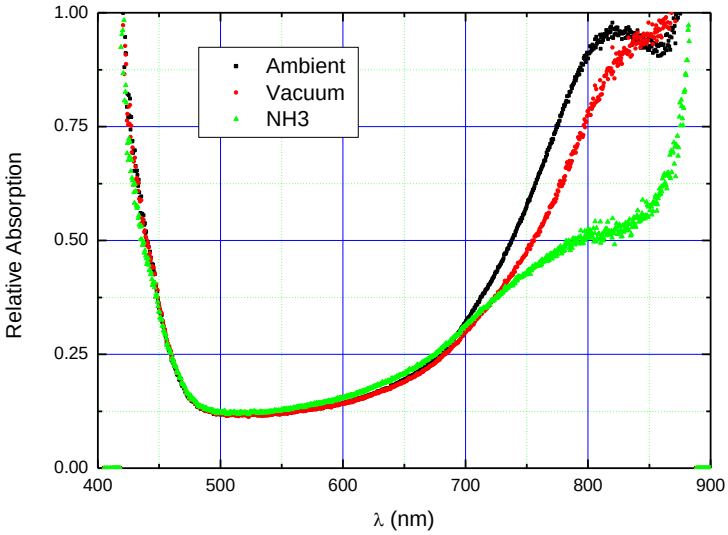

Figure 5. Optical absorption of a green film (G1) in ambient conditions, in vacuum and at 500 ppm of NH_3.

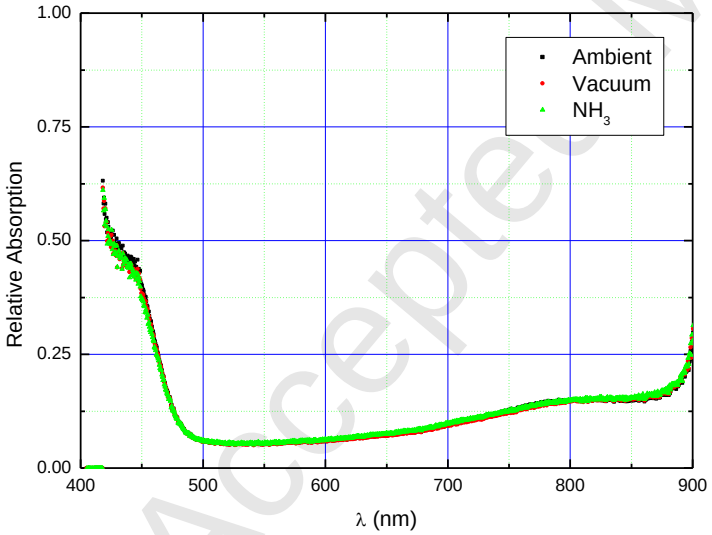

Figure 6. Optical absorption of a yellow film (Y1) in ambient conditions, in vacuum and at 500 ppm of NH_3.

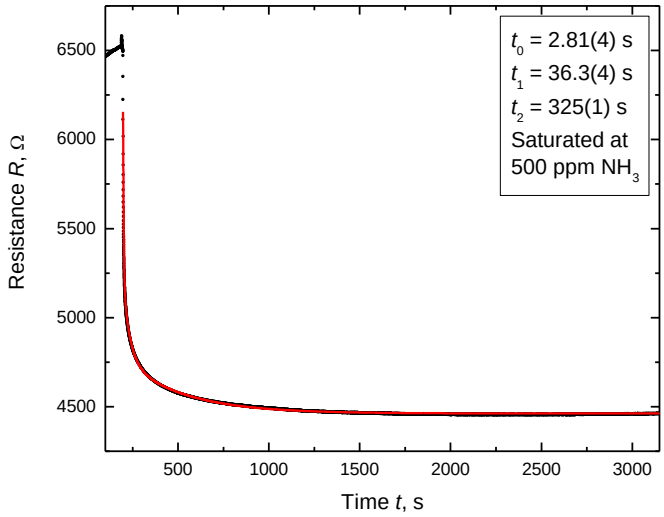

Figure 7. The dynamic ammonia desorption response of the resistance of a PAni film and a three exponent fit to it.

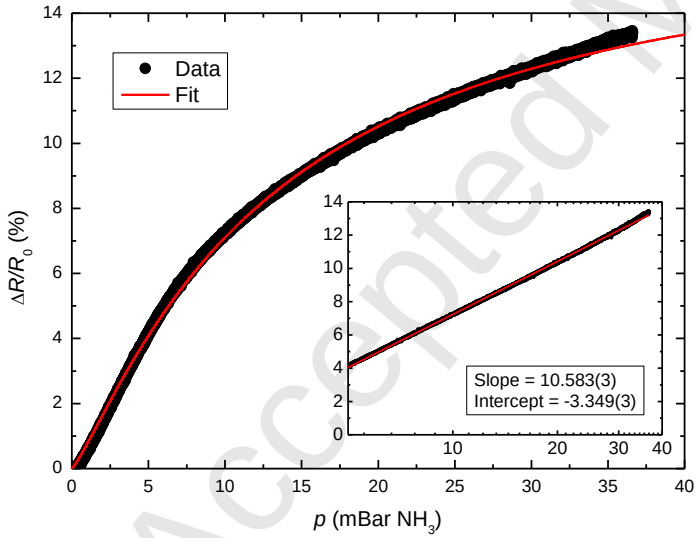

Figure 8. Typical slow, close to equilibrium, response of doped-PAni (HBr) and a fit to it. The dependence is verified to be logarithmic at high ammonia concentrations as shown on the inset.

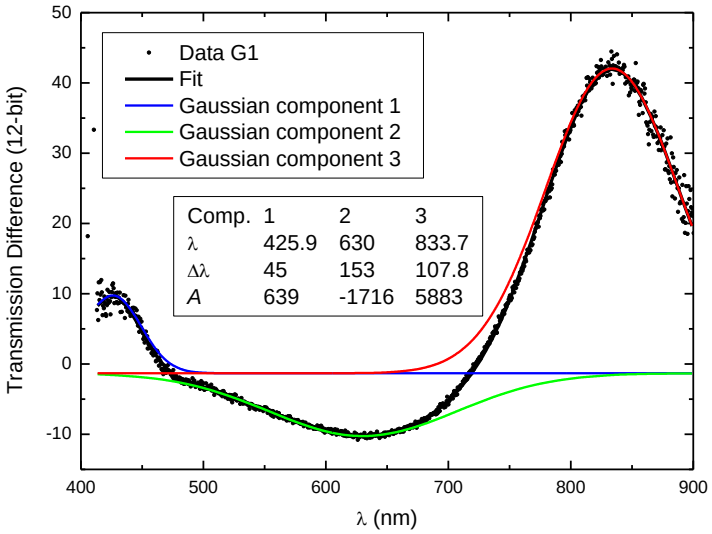

Figure 9. Difference of the equilibrium absorption spectra of the HCl-doped before and after exposure to 500 ppm ammonia. (check) The fit of the difference to three Gaussian components centred at 440 nm, 650 nm and 840 nm is shown.

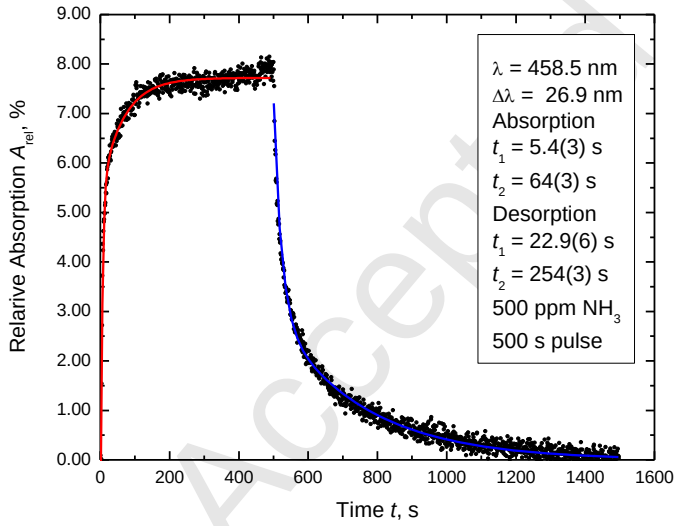

Figure 10. Fits to the time-dependent absorption and desorption response of the intensity of the spatial component centred at 459 nm for sample Y3.

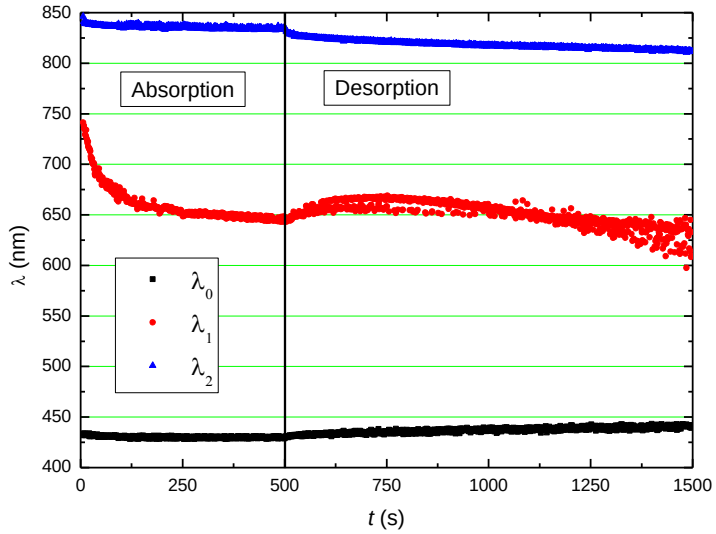

Figure 11. An example of the temporal evolution of the fitted spectral components' positions (ammonia absorption, 500 ppm – for sample G2), with its constituent components.

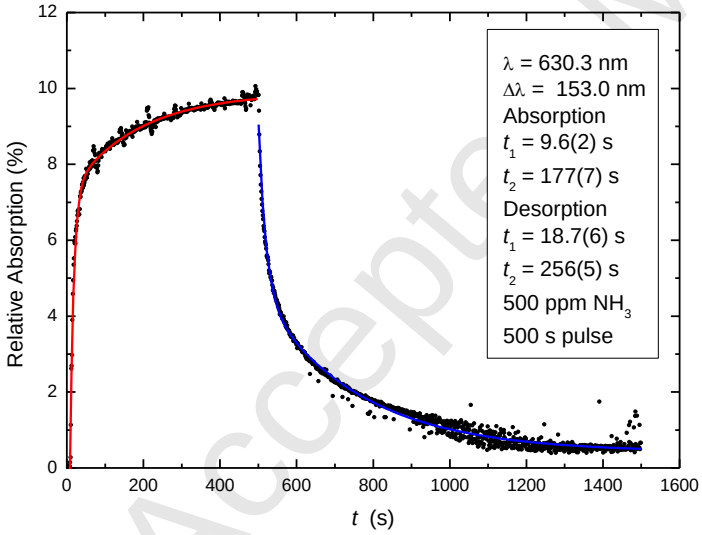

Figure 12. Fits to the time-dependent absorption and desorption response of the intensity of the spatial component centred at 630 nm for sample G1.

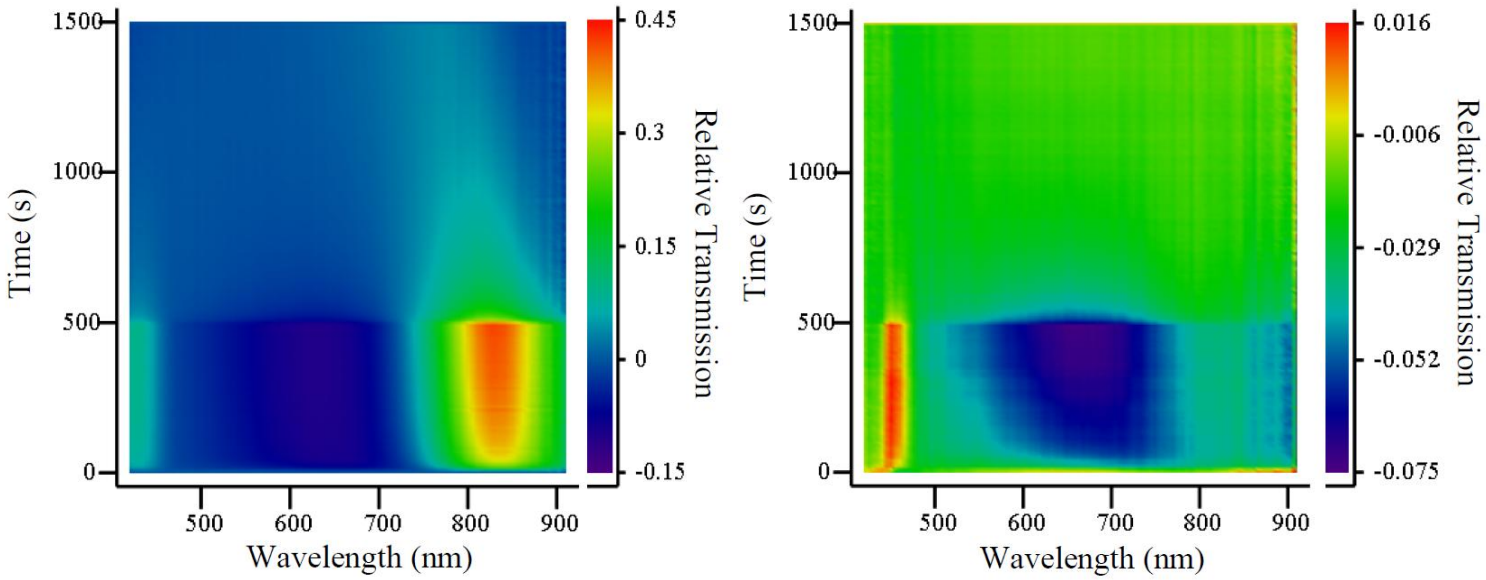

Figure 13. Time dependent optical transmission of a green film (G1 – left panel) and a yellow film (Y1 – right panel) when subjected to a 500 seconds pulse of 500 ppm of NH_3.

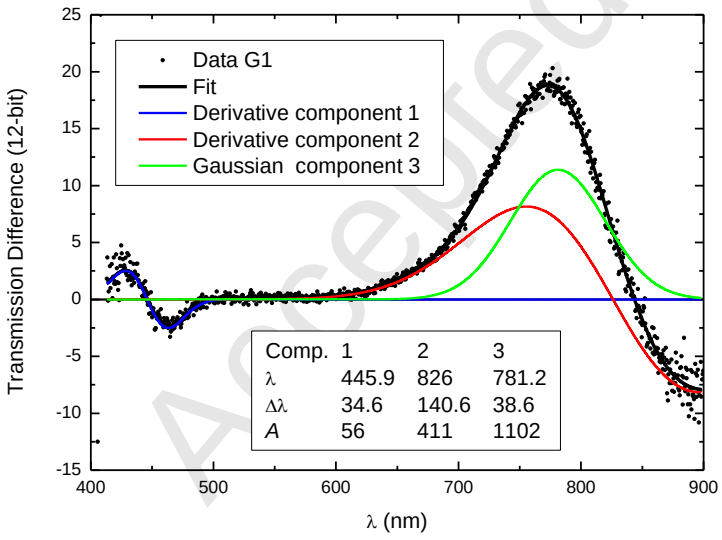

Fig. 14. An example of a fit to the difference spectrum (vacuum - air) for sample G1, with its constituent components.

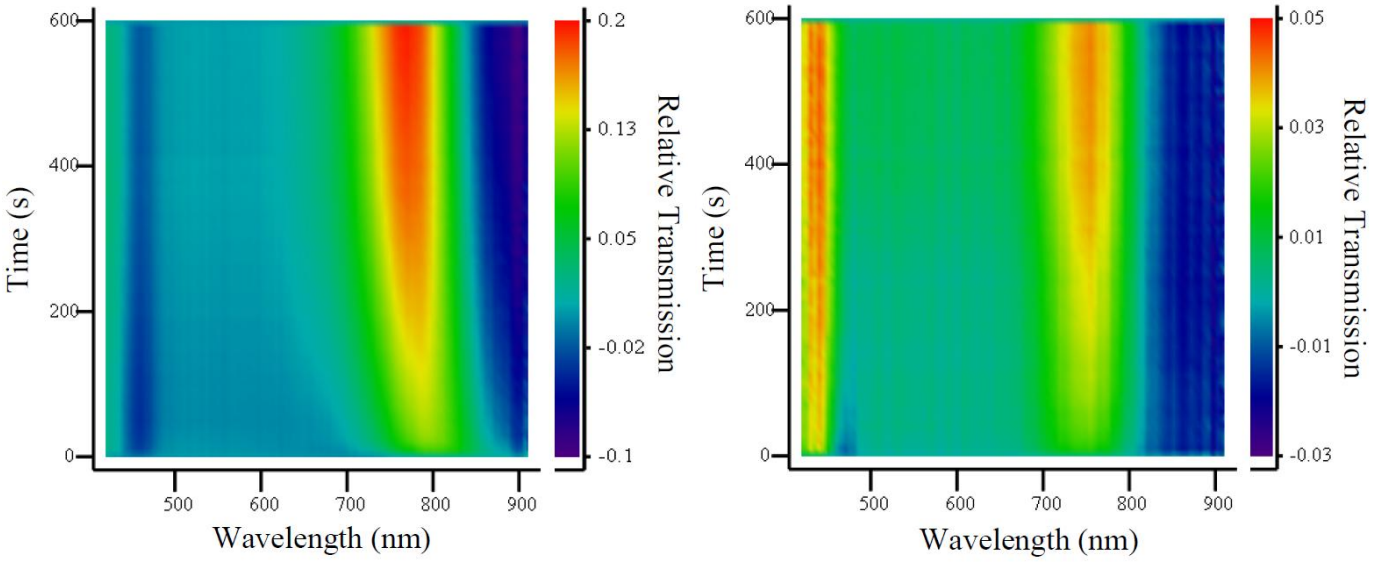

Figure 15. Time dependent optical transmission of a green film (G1 – left panel) and a yellow film (Y1 – right panel) when subjected to vacuum (p < 5 10^{-3} mBar), starting from ambient conditions.

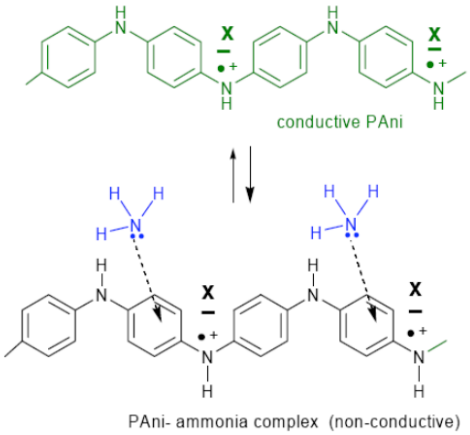

Figure 16. Interaction of ammonia with polyaniline.

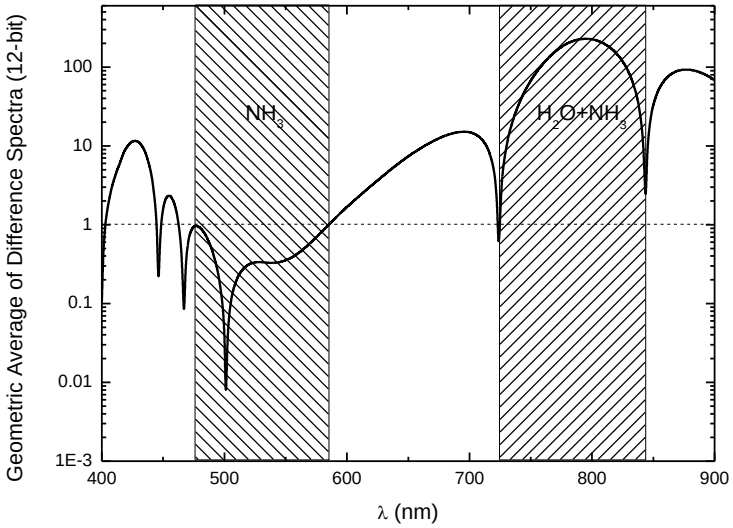

Fig 17. Geometric average of the difference spectra for NH_3 and H_2O. The shaded regions show the spectral regions of the suggested band-pass filters that can be used for sensing and discrimination of NH_3 and H_2O vapours.

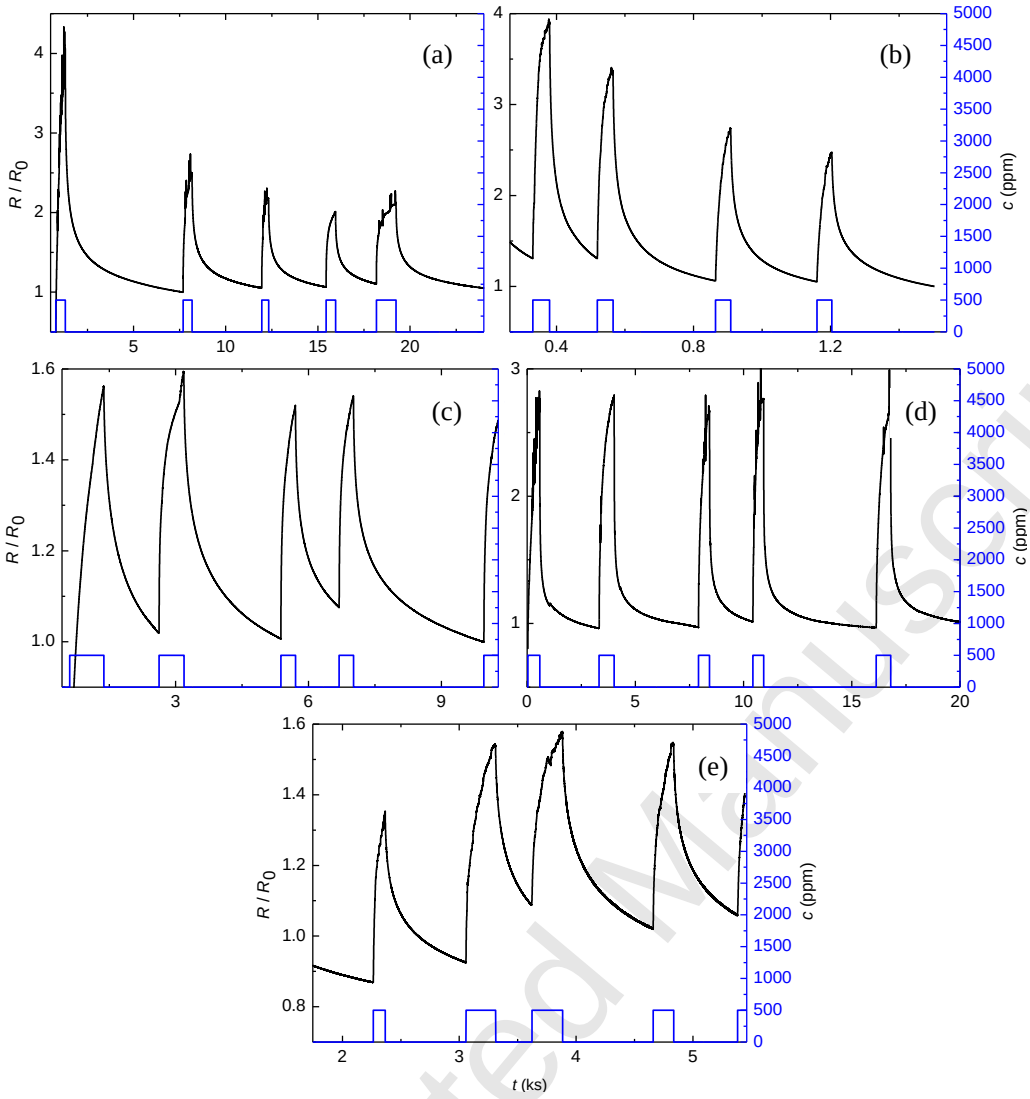

Figure A1. Examples of the resistive response of polianiline films with different acid doping, (a – HCl, b – $HClO_4$, c – HNO_3, d – H_2SO_4, e - HBr) upon repeated pulsing with ammonia gas at concentrations of about 500 ppm. The corresponding R_0 values are (18.2 K, 3.6 K, 23.7 K, 2.3 K, 18.1 K).